ARM TR-047

# Cloud Optical Properties from the Multi-Filter Shadowband Radiometer (MFRSRCLDOD): An ARM Value-Added Product

December 2004

David D. Turner
Chaomei Lo
Pacific Northwest National Laboratory – Richland, Washington

Qilong Min
State University of New York (SUNY) – Albany, New York

Work supported by the U.S. Department of Energy,
Office of Science, Office of Biological and Environmental Research

## Contents



## Figures



## Tables

## 1. Introduction

The microphysical properties of clouds play an important role in studies of global climate change. Observations from satellites and surface-based systems have been used to infer cloud optical depth and effective radius. Min and Harrison (1996) developed an inversion method to infer the optical depth of liquid water clouds from narrow band spectral multi-filter rotating shadowband radiometer (MFRSR) measurements (Harrison et al. 1994). Their retrieval also uses the total liquid water path (LWP) measured by a microwave radiometer (MWR) to obtain the effective radius of the warm cloud droplets. Their results were compared with Geostationary Operational Environmental Satellite (GOES) retrieved values at the Atmospheric Radiation Measurement (ARM) Southern Great Plains (SGP) site (Min and Harrison 1996). Min et al. (2003) also validated the retrieved cloud optical properties against in situ observations, showing that the retrieved cloud effective radius agreed well with the in situ forward scattering spectrometer probe (FSSP) observations. The retrieved cloud optical properties from Min et al. (2003) were used also as inputs to an atmospheric shortwave model, and the computed fluxes were compared with surface pyranometer observations.

The Min and Harrison algorithm has been incorporated into an ARM Value-Added Product (VAP) called MFRSR CLDOD. This version of the VAP (1Min) uses the diffuse transmission at 415 nm from the MFRSR. Therefore, the results are only valid for "horizontally homogeneous" stratiform clouds with optical depths larger than approximately 7. The retrieval assumes a single cloud layer consisting solely of liquid water drops. As specified by Min and Harrison (1996), the wavelength at 415 nm was chosen due to the lack of gaseous absorption and the relatively constant surface albedo (in the absence of snow) at this wavelength.

The MFRSR CLDOD VAP (henceforth referred to as "the VAP") retrieves cloud optical depth ($\tau$) from the MFRSR measurements. If the LWP is available from a coincident MWR observation, then the droplet effective radius ($r_e$) can be determined. Knowledge of the estimated $r_e$ can be used to improve the estimate of $\tau$ because there is a slight dependence on the extinction coefficient, single scattering albedo, and asymmetry parameter on effective radius at this wavelength. However, if the MWR's LWP is not available, then the VAP assumes that $r_e = 8.0$ μm. The primary output from the VAP is $\tau$ and $r_e$.

The VAP also provides 1-sigma uncertainties for $\tau$ and $r_e$ by propagating the uncertainties in the top-of-atmosphere irradiance ($I_0$), the measured irradiance (I), the MWR's LWP, and the surface albedo.

## 2. Input Data

The input files for this VAP are standard ARM NetCDF products. To run this VAP properly, we need the following input files and data for the SGP site:[1]

**Multi-Filter Rotating Shadowband Radiometer instrument:**

sgpmfrsrE13.b1 – 20 s data

This data stream contains the observed irradiance data (I) from the MFRSR.

[1] For details of the input variables, see Appendix A.

**Microwave Radiometer instruments:**

sgpmwrlosC1.a1

The LWP from the MWR.

**Langley Value Added Project:**

sgpmfrsrLangleyE13.c1 – 2 data points per day

This VAP provides the top of atmosphere irradiance ($I_0$) data.

**Short Wave Flux Value Added Project:**

sgp15swfanalsirs1longC1.c1

This VAP provides ancillary data for future analyses regarding the cloud sky cover fraction.

**Cloud Base Height Value Added Project:**

sgparsclbnd1clothC1.c1

This VAP provides ancillary data for future analyses regarding the height (and by inference the phase) of the clouds.

## 3. Output Data

The name of the output file is:

sgpMFRSRCldOD1MinE13.C1.YYYYMMDD.hhmmss – 20 s data

Where:

| | | |
|---|---|---|
| SGP | – | the site of the instrument |
| MFRSR | – | the main instrument name |
| CldOD1Min | – | identifies that this is Min's version 1 VAP |
| E13 | – | facility |
| YYYY | – | year, MM - month of the year, DD - day of the month, hh - hour of the day, mm - minute of the hour, ss - second of the minute of data start |

The detailed variable description is in Table 2 of Appendix B.

This VAP generates two quicklook plots: one is the $I_0$ calibration in Figure 1 and the second is the cloud optical properties in Figure 4. The names of the quicklook files are

YYYYMMDD_quicklook.png

Io_YYYYMMDD_quicklook.png

## 4. Algorithm/Method

The functioning heart of this VAP is the Nonlinear Least Squares retrieval algorithm of Min and Harrison (1996). This algorithm uses a parameterization of the scattering properties at 415 nm on the effective radius and LWP using Mie theory. The algorithm uses an adjoint formulation of the radiative transfer to maintain accuracy and improve its execution speed. It uses an iterative approach to retrieve both cloud optical depth and effective radius if an estimate of LWP is provided; otherwise the effective radius is assumed and the algorithm returns only optical depth.

The algorithm requires the atmospheric transmittance at 415 nm. This is easily computed using the observed irradiance I and the top of the atmosphere irradiance $I_0$, where $I_0$ is computed from Langley regressions on clear days. Because data from the MFRSR are used to obtain both I and $I_0$, the absolute calibration of the instrument is not required to get accurate observations of the atmospheric transmittance.

A previously developed VAP routinely analyzed the MFRSR data and computes $I_0$. However, the most accurate values of $I_0$ are obtained only on days that are free of clouds and stable. Furthermore, a maximum of two Langley regressions could be computed for a single day. Because this VAP is concerned with cloud properties, the $I_0$ values used are computed from $I_0$ values determined on nearby clear sky days. We have automated a procedure to determine an accurate value of $I_0$. The VAP reads in all of the $I_0$ data that were determined to be good by the Langley analysis VAP for 3 months before and after the day currently being processed. From this large dataset, we select the 20 closest in time $I_0$ values. We then follow the procedure outlined in Michalsky et al. (2001) to select the best 10 of the 20 points; the mean value of these 10 points is used as the $I_0$ for the processing. The uncertainty in $I_0$ represented by the standard deviation about the mean $I_0$ value of the 10 points is propagated to provide uncertainties in the retrieved cloud properties. Figure 1 shows a quicklook plot that displays all of the $I_0$ values determined by the Langley algorithm VAP, the 20 closest points, and the mean and standard deviation of the $I_0$ value used in the VAP.

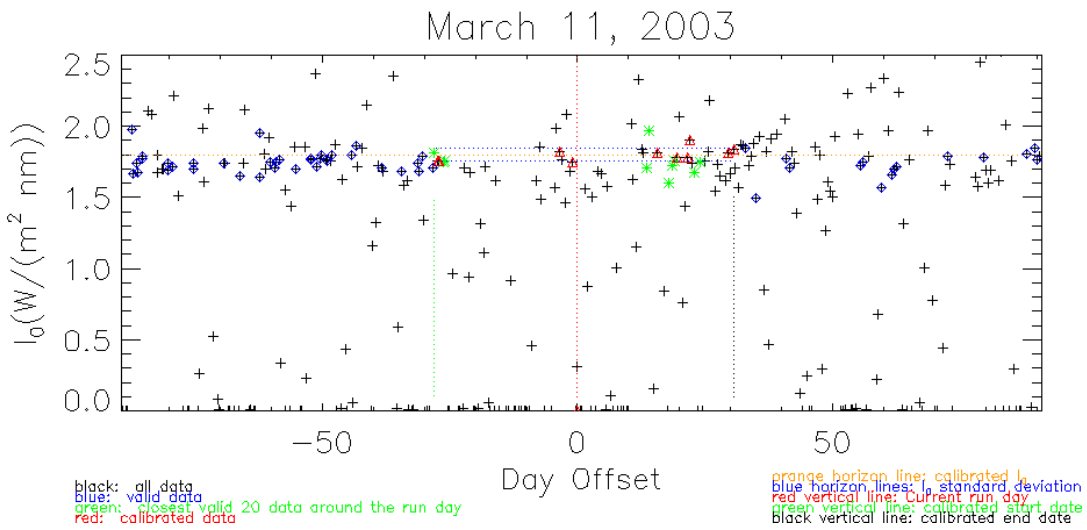


**Figure 1.** $I_0$ Calibration quicklook plot. See text for details.

The LWP from the MWR, while not critical for the execution of the VAP, does permit the retrieval of effective radius. The VAP applies some simple quality control to ensure that the reported LWP is valid. If the observed brightness temperature at either MWR frequency is below the cosmic background or above 100K (the latter condition is usually indicative of rain) then the LWP value from the MWR is not used in the retrieval. Furthermore, because the uncertainty in the MWR's retrieval LWP is approximately 20 g m$^{-2}$ (Westwater et al. 2001), the VAP does not use the MWR's observed LWP in the retrieval if the LWP is below this threshold. When no LWP is available, the retrieval algorithm assumes that the effective radius is 8 μm.

The temporal resolution of the MFRSR irradiance data is 20 s, and therefore the ancillary inputs are interpolated to this time. The interpolation of the LWP is usually required. The LWP is interpolated across gaps of a maximum of 5 min. If the temporal gap is larger than this, then the retrieval is run without LWP input for those MFRSR samples.

Because this VAP can be run at sites that has a MFRSR, such as the ARM extended facilities, the VAP uses the retrieved optical depth and assumed effective radius to provide an estimate of the LWP using

$$LWP = (2/3) * \rho * \tau * r_e$$

Where ρ is the density of liquid water, τ is retrieved by the VAP, and $r_e$ was assumed. This provides estimates of the LWP at sites where MWRs are not deployed. However, due to the natural variability in $r_e$ the uncertainty in this derived LWP is large. A flag is set in the output file to indicate if the output LWP is from the MWR or this calculation.

The retrieval algorithm operates at two temporal resolutions. It provides "instantaneous" retrievals at the nominal 20 s resolution of the MFRSR and "average" retrievals where the data have been averaged for 5 min centered upon the ouput sample time. The average retrievals are less sensitive to the spatial inhomogenialties in the cloud, which affect the diffuse irradiance field.

As indicated above, the VAP provides 1-sigma uncertainties for both the retrieved optical depth and effective radius by propagating the uncertainties in the input and assumed parameters. The uncertainty in the $I_0$ value is the standard deviation about the mean $I_0$ as described above. If the LWP is available from the MWR, the uncertainty in the LWP is assumed to be 20 g $m^{-2}$. The uncertainty in the observed irradiance is assumed to be 1%. The surface albedo, which is taken to be 0.036 at 415 nm in non-snow covered conditions, is assumed to have an uncertainty of ±0.01. These uncertainties are propagated individually using finite differences and combined as the root sum of squared errors (i.e., these uncertainties are assumed to be independent). The uncertainty in the retrieved optical depth is dominated by the uncertainty in $I_0$, while the uncertainty in the LWP is the dominant term in the effective radius uncertainty. Figures 2 and 3 present examples of distributions of each component of the total uncertainty to the uncertainty in $\tau$ and $r_e$, respectively, as well as the distributions of the total uncertainty in each retrieved variable for data from the SGP site over a 6-month period.

Finally, this VAP provides some ancillary data to help the analyst find cases where the retrieval is valid. The fractional sky cover from the shortwave analysis VAP (Long and Gaustad 2004) is included because the retrievals from this VAP are only valid in overcast scenes. The cloud base height from the active remote sensing clouds (ARSCL) VAP (Clothiaux et al. 2001), along with the infrared thermometer (IRT) sky brightness temperature, are included because the retrievals are also only valid for single layer liquid water clouds. Therefore, the user should use these fields to help select the proper cases to analyze.

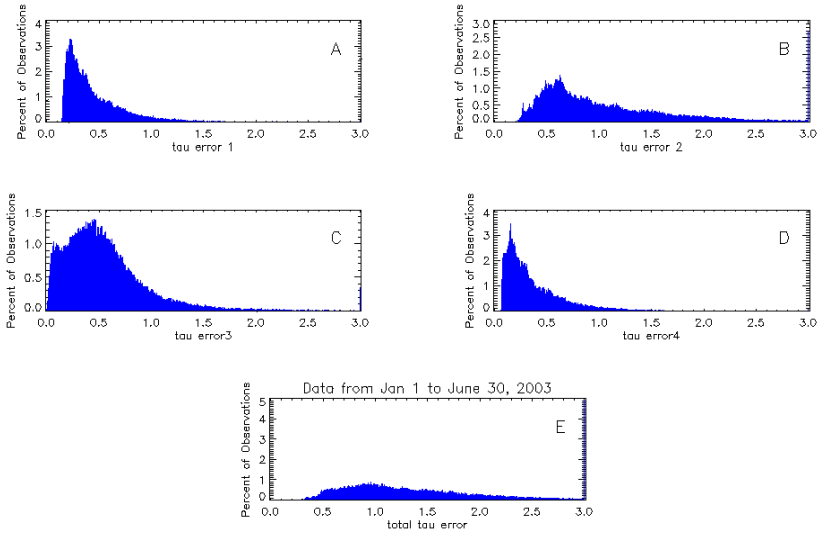


**Figure 2.** Distribution of the uncertainties in cloud optical depth for uncertainties in A) I, B) $I_0$, C) LWP, D) surface albedo. Panel E shows the distribution of the total uncertainty in the cloud optical depth for this 6-month period (Jan – Jun 2003)

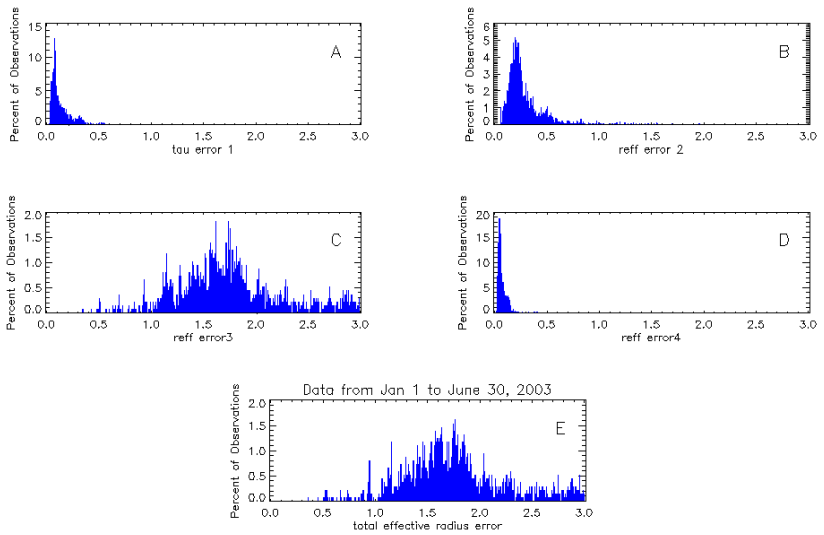


**Figure 3.** Distribution of the uncertainties in effective radius for uncertainties in I, B) $I_0$, C) LWP, D) surface albedo. Panel E shows the distribution of the total uncertainty in the cloud optical depth for this 6-month period (Jan – Jun 2003)

## 5. Examples

This VAP runs on the daily basis. There are two quicklook plots generated everyday, one is the $I_0$ calibration in Figure 1 as explained before and the other one is a five-panel plot for the cloud properties. Figure 4 gives an example for March 11, 2003. The data start around 13:50 Universal Time Coordinates (UTC) and ends around 24:00. An overcast liquid water cloud persisted on this day, as the clouds were of low height and the effective radius was small indicating the presence small cloud drops. The first panel shows the derived cloud optical depth data for instantaneous (20 s) and averaged (5-min) resolutions. The second panel shows the retrieved effective radius. The third panel shows the ratios of the total uncertainty to the retrieved data. Panel four displays the cloud fraction and cloud height. The last panel shows the LWP from MWR or the LWP from the default effective radius (which it does not have on this day, because all of the MWR LWP data were valid).

The six months of data from January 1 to June 30, 2003, are show in Figure 5 and the distributions of the cloud properties for this period are shown in Figure 6. Only valid data meeting the following criterion are included in Figures 5 and 6. The criteria are cloud fraction > 90 %, infrared temperature > 268 (-50°C), cloud base height < 4 km, optical depth > 7, effective radius ≠ 8.00 μm (because an effective radius equal to 8 μm implies that the LWP from the MWR was not available or not used), and effective radius > 0.

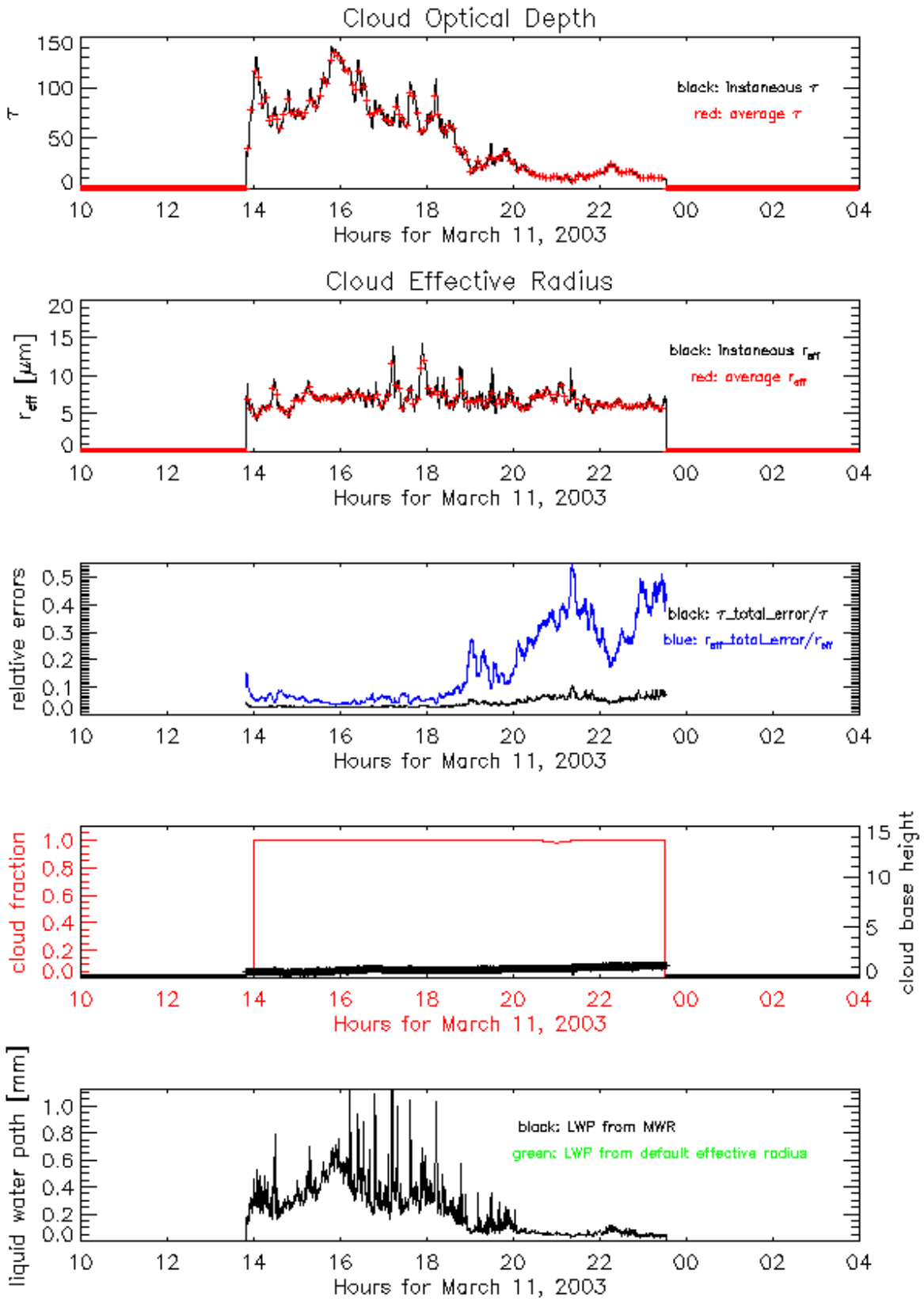


**Figure 4.** Quicklook image showing the cloud optical properties for March 11, 2003

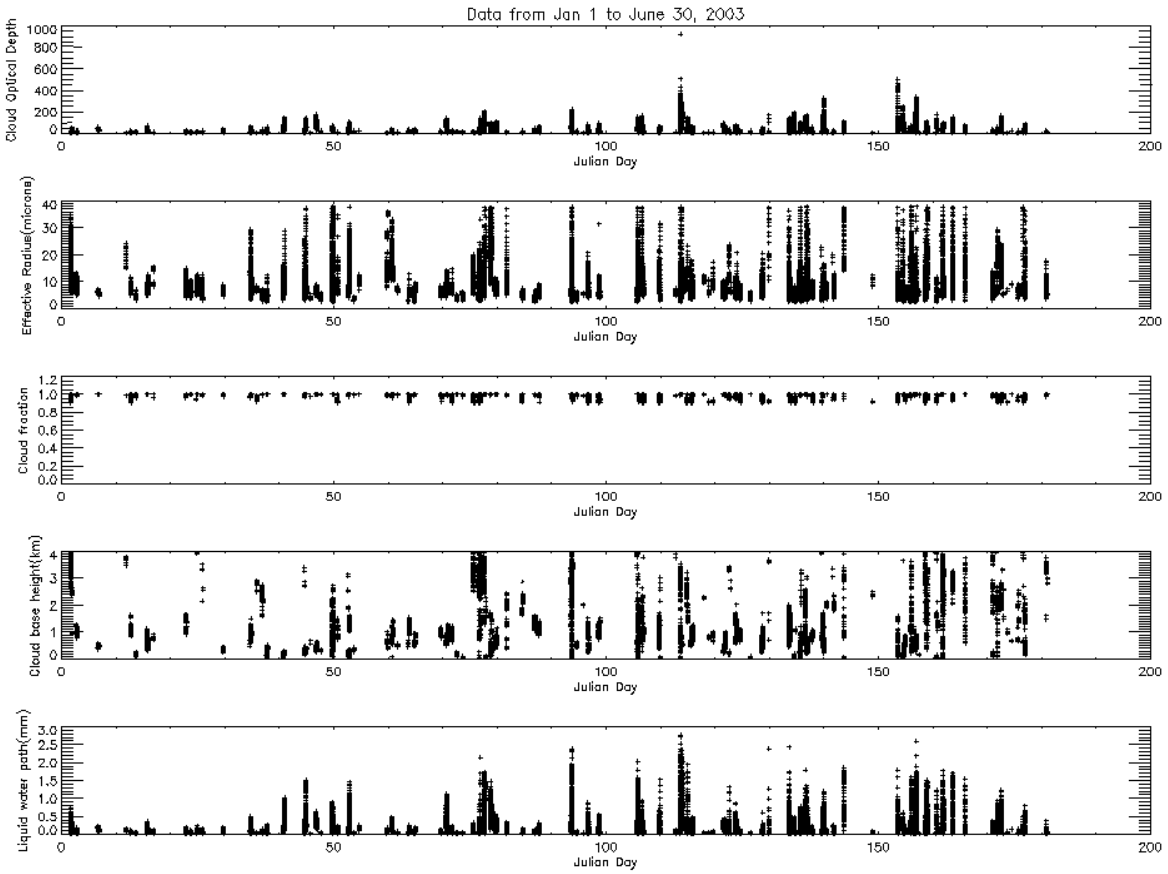


**Figure 5.** Retrieved cloud optical properties for 6 months of data starting 1 Jan 2003. A) retrieved τ, B) retrieved $r_e$, C) cloud fraction from shortwave flux analysis VAP, D) cloud base height from ARSCL VAP, E) LWP from the MWR.

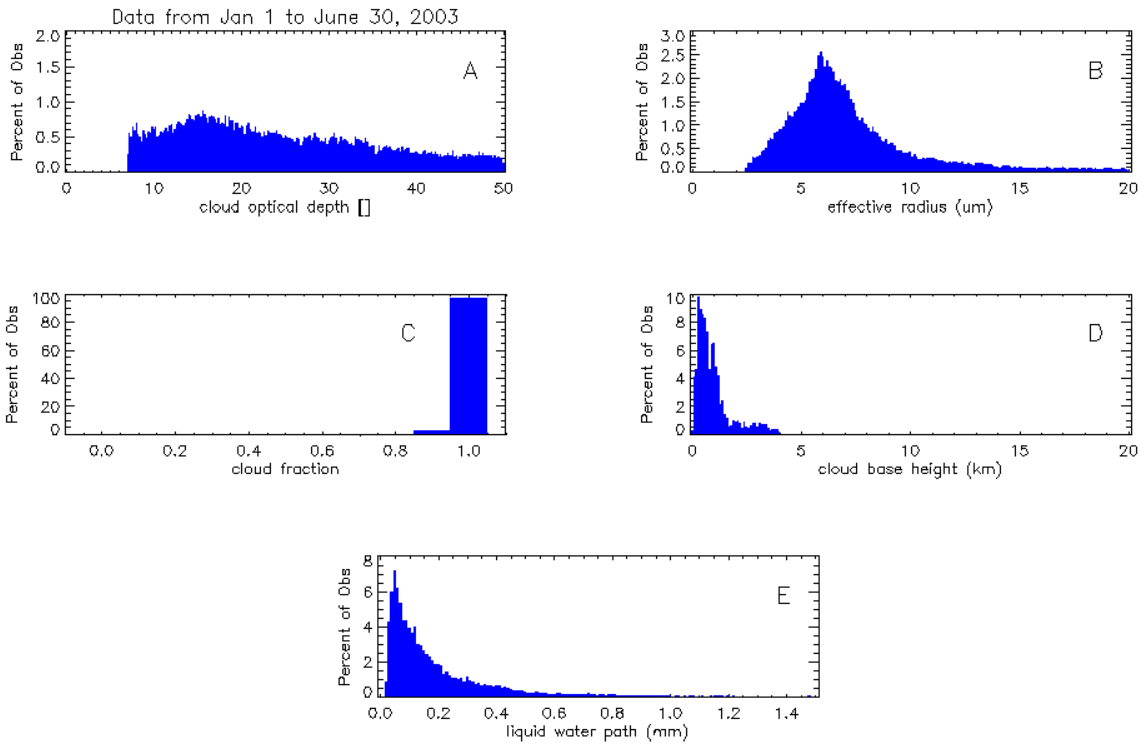


**Figure 6.** Distributions of the retrieved cloud optical depth (A) and effective radius (B) from 1 Jan to 30 June 2003. Panel C, D and E show the corresponding cloud fraction, cloud height and LWP

## 6. Known Caveats

- Only valid for overcast conditions where cloud is liquid. Because there is no gaseous absorption at this wavelength (415 nm), the retrieval will be valid for both single layer and multiple layer cloud conditions, as long as all layers are overcast and composed entirely of liquid drops.

- Assumes the surface is not covered with snow or ice.

- Biases in the MWR's LWP, especially for small optical depths, will bias the retrieved effective radius.

## 7. References

Clothiaux, EE., MA Miller, RC Perez, DD Turner, KP Moran, BE Martner, TP Ackerman, GG Mace, RT Marchand, KB Widener, DJ Rodriguez, T Uttal, JH Mather, CJ Flynn, KL Gaustad, and B Ermold. 2001. The ARM millimeter wave cloud radars (MMCRs) and the active remote sensing of clouds (ARSCL) Value Added Product (VAP). ARM-TR-002-1. U.S. Department of Energy. Available at http://www.arm.gov/publications/tech_reports/armvap-002-1.pdf.

Harrison, LC, JJ Michalsky, and J Berndt. 1994. "Automated multi-filter rotating shadowband radiometer: an instrument for optical depth and radiation measurements." *Applied Optics* 33:5126-5132.

Long, CN, and KLGaustad. 2004. The shortwave (SW) clear-sky detection and fitting algorithm: algorithm operational details and explanations. Revision 1. ARM-TR-004-1. U.S. Department of Energy. Available at http://www.arm.gov/publications/tech_reports/arm-tr-004-1.pdf.

Michalsky, JJ, JA Schlemmer, WE Berkheiser, JL Berndt, LC Harrison, NS Laulainen, NR Larson, and JC Barnard. 2001. "Multiyear measurements of aerosol optical depth in the Atmospheric Radiation Measurement and Quantitative Links programs." *Journal of Geophysical Research* 106:12099-12107.

Min, Q and LC Harrison. 1996. "Cloud properties derived from surface MFRSR measurements and comparison with GOES results at the ARM SGP site." *Geophysical Research Letters* 23:1641-1644.

Min, Q, M Duan, and R Marchand. 2003. "Validation of surface retrieved cloud optical properties with in situ measurements at the Atmospheric Radiation Measurement Program (ARM) South Great Plains site." *Journal of Geophysical Research* 108, 4547, doi:10.1029/2003JD003385.

Westwater,E.R., Y Han, MD Shupe, SY Matrosov. 2001. "Analysis of integrated cloud liquid and precipitable water vapor retrievals from MWRs during SHEBA." *Journal of Geophysical.Res*earch 106: 32,019-32,030.

# Appendix A - Input Data

Table 1 lists the various ARM data streams used in the VAP for data, along with the specific variables in files that are used in processing.

**Table 1.** Input Variables

| Data Stream | Variable Name | Variable Long Name | Units |
|---|---|---|---|
| **sgpmfrsrE13.b1** | cosine_solar_zenith_angle | Cosine Solar Zenith Angle | unitless |
| | hemisp_narrowband_filter1 | Narrowband Hemispheric Irradiance, Filter 1 | W/(m$^2$ nm) |
| | hemisp_narrowband_filter2 | Narrowband Hemispheric Irradiance, Filter 2 | W/(m$^2$ nm) |
| | hemisp_narrowband_filter3 | Narrowband Hemispheric Irradiance, Filter 3 | W/(m$^2$ nm) |
| | hemisp_narrowband_filter4 | Narrowband Hemispheric Irradiance, Filter 4 | W/(m$^2$ nm) |
| | hemisp_narrowband_filter5 | Narrowband Hemispheric Irradiance, Filter 5 | W/(m$^2$ nm) |
| | direct_normal_narrowband_filter1 | Narrowband Direct Normal Irradiance, Filter 1 | W/(m$^2$ nm) |
| | direct_normal_narrowband_filter2 | Narrowband Direct Normal Irradiance, Filter 2 | W/(m$^2$ nm) |
| | direct_normal_narrowband_filter3 | Narrowband Direct Normal Irradiance, Filter 3 | W/(m$^2$ nm) |
| | direct_normal_narrowband_filter4 | Narrowband Direct Normal Irradiance, Filter 4 | W/(m$^2$ nm) |
| | direct_normal_narrowband_filter5 | Narrowband Direct Normal Irradiance, Filter 5 | W/(m$^2$ nm) |
| **sgpmwrlosC1.b1** | vap | Total water vapor along LOS path | cm |
| | liq | Total liquid water along LOS path | cm |
| | tbsky23 | 23.8 GHz sky brightness temperature | K |
| | tbsky31 | 31.4 GHz sky brightness temperature | K |
| | sky_ir_temp | IR Brightness Temperature | K |
| **sgpmfrsrlangleyE13.c1** | barnard_solar_constant_sdist_filter1 | solar constant corrected for solar distance for the Direct Narrowb and Filter 1 | W/(m$^2$ nm) |
| | barnard_solar_constant_sdist_filter2 | solar constant corrected for solar distance for the Direct Narrowb and Filter 2 | W/(m$^2$ nm) |
| | barnard_solar_constant_sdist_filter3 | solar constant corrected for solar distance for the Direct Narrowb and Filter 3 | W/(m$^2$ nm) |
| | barnard_solar_constant_sdist_filter4 | solar constant corrected for solar distance for the Direct Narrowb and Filter 4 | W/(m$^2$ nm) |
| | barnard_solar_constant_sdist_filter5 | solar constant corrected for solar distance for the Direct Narrowb and Filter 5 | W/(m$^2$ nm) |
| | barnard_badflag_filter1 | rejection flag for Direct Narrowband Filter 1 | unitless |
| | barnard_badflag_filter2 | rejection flag for Direct Narrowband Filter 2 | unitless |
| | barnard_badflag_filter3 | rejection flag for Direct Narrowband Filter 3 | unitless |
| | barnard_badflag_filter4 | rejection flag for Direct Narrowband Filter 4 | unitless |
| | barnard_badflag_filter5 | rejection flag for Direct Narrowband Filter 5 | unitless |
| **sgp15swfanalsirs1longC1.c1** | cloudfraction | Estimated Average Fractional Sky Cover over the Hemispheric Dome (cf) | unitless |
| **sgparsclbnd1clothC1.c1** | cloudbasebestestimate | LASER Cloud Base Height Best Estimate | m AGL |

# Appendix B - Output Variables

Table 2 lists the detail description of the variables for the MFRSRCLDOD1MIN VAP output file.

Table 2. Output Variables

| Fieldname | Description | Units |
|---|---|---|
| base_time | Base Time in Epoch | seconds since 1970/01/01 00:00:00 |
| time_offset | Time offset from base_time | seconds since base_time |
| time | Time offset from midnight | seconds since midnight |
| optical_depth_instaneous | Cloud Optical Depth (Instaneous | unitless |
| effective_radius_instaneous | Effective Radius (Instaneous) | microns |
| optical_depth_average | Cloud Optical Depth (Average) | unitless |
| effective_radius_average | Effective Radius (Average) | microns |
| cldtaui_error1 | Cloud Taui Error1 (1% uncertainty in total irradiance) | unitless |
| cldtaui_error2 | Cloud Taui Error2 (5% uncertainty in Inought) | unitless |
| cldtaui_error3 | Cloud Taui Error3 (uncertainty in liquid water path (LWP) 0.015mm larger) | unitless |
| cldtaui_error4 | Cloud Taui Error4 (20% uncertainty in surface albedo) | unitless |
| cldtaui_error5 | Cloud Taui Error5 (uncertainty in 3um higher of effective radius when there is no MWR data) | unitless |
| cldtaui_toterror | Instantaneous Cloud Tau Total Uncertainty | unitless |
| cldtaua_error1 | Cloud Taua Error1 (1% uncertainty in total irradiance) | unitless |
| cldtaua_error2 | Cloud Taua Error2 (5% uncertainty in Inought) | unitless |
| cldtaua_error3 | Cloud Taua Error3 (uncertainty in liquid water path (LWP) 0.015mm larger) | unitless |
| cldtaua_error4 | Cloud Taua Error4 (20% uncertainty in surface albedo) | unitless |
| cldtaua_toterror | Average Cloud Tau Total Uncertainty | unitless |
| reffi_error1 | Effective Radiusi Error1 (1% uncertainty in total irradiance) | microns |
| reffi_error2 | Effective Radiusi Error2 (uncertainty is standard deviation of calibrated 10 Inought points) | microns |
| reffi_error3 | Effective Radiusi Error3 (uncertainty in liquid water path (LWP) 0.001mm larger, using scaling factor with 0.015 mm) | microns |
| reffi_error4 | Effective Radiusi Error4 (uncertainty is 0.01 in surface albedo) | microns |
| reffi_toterror | Instaneouse Effective Radius Total Error | microns |
| reffa_error1 | Effective Radiusa Error1 (1% uncertainty in total irradiance) | microns |
| reffa_error2 | Effective Radiusa Error2 (uncertainty is standard deviation of calibrated 10 Inought points) | microns |
| reffa_error3 | Effective Radiusa Error3 (uncertainty in liquid water path (LWP) 0.001mm larger, using scaling factor with 0.015 mm) | microns |
| reffa_error4 | Effective Radiusa Error4 (uncertainty is 0.01 in surface albedo) | microns |
| reffa_toterror | Average Effective Radius Total Error | microns |
| cosine_solar_zenith_angle | Cosine Solar Zenith Angle | unitless |
| total_transmittance_filter1 | Diffuse Transmission of Narrowband Hemispheric Irradiance, Filter 1 | unitless |
| total_transmittance_filter2 | Diffuse Transmission of Narrowband Hemispheric Irradiance, Filter 2 | unitless |
| total_transmittance_filter3 | Diffuse Transmission of Narrowband Hemispheric Irradiance, Filter 3 | unitless |
| total_transmittance_filter4 | Diffuse Transmission of Narrowband Hemispheric Irradiance, Filter 4 | unitless |
| total_transmittance_filter5 | Diffuse Transmission of Narrowband Hemispheric Irradiance, Filter 5 | unitless |

**Table 2.** (cont'd)

| Fieldname | Description | Units |
|---|---|---|
| direct_transmittance_filter1 | Direct tranmittance of Narrowband Direct Normal Irradiance, Filter 1 | unitless |
| direct_transmittance_filter2 | Direct tranmittance of Narrowband Direct Normal Irradiance, Filter 2 | unitless |
| direct_transmittance_filter3 | Direct tranmittance of Narrowband Direct Normal Irradiance, Filter 3 | unitless |
| direct_transmittance_filter4 | Direct tranmittance of Narrowband Direct Normal Irradiance, Filter 4 | unitless |
| direct_transmittance_filter5 | Direct tranmittance of Narrowband Direct Normal Irradiance, Filter 5 | unitless |
| pwv | Total water vapor along MWR LOS path | cm |
| lwp | Total liquid water along LOS path, it could come from either MWR or the MFRSR with an assumed effective radius | mm |
| ir_temp | IR Brightness Temperature | K |
| cloudfraction | Estimated Average Fractional Sky Cover over the Hemispheric Dome (cf) | unitless |
| cloudbasebestestimate | Cloud Base Height Best Estimate | m AGL |
| lwp_uncertainty | LWP uncertainty if derived from MFRSR | mm |
| lwp_source | LWP Source, =1 from MWR, =2 from MFRSR data, =0 from other | unitless |
| Io_time | Langley time series | Day fraction offset from 00:00 on this day |
| Io_filter1 | solar constant corrected for solar distance for the Direct Narrowb and Filter1 | W/(m$^2$ nm) |
| Io_filter2 | solar constant corrected for solar distance for the Direct Narrowb and Filter2 | W/(m$^2$ nm) |
| Io_filter3 | solar constant corrected for solar distance for the Direct Narrowb and Filter3 | W/(m$^2$ nm) |
| Io_filter4 | solar constant corrected for solar distance for the Direct Narrowb and Filter4 | W/(m$^2$ nm) |
| Io_filter5 | solar constant corrected for solar distance for the Direct Narrowb and Filter5 | W/(m$^2$ nm) |
| Io_flag_filter1 | Inought flag rejection flag for Direct Narrowband Filter1 | unitless |
| Io_filter1_final | The final Inought that used to determine total transmission | W/(m$^2$ nm) |
| cal_start_date | Start day for the Io data selected for calibration | Day fraction offset from 00:00 on this day |
| cal_end_date | End day for the Io data selected for calibration | Day fraction offset from 00:00 on this day |
| Io_filter1_standard_deviation | Standard deviation of Inought to the closest 10 points around the run day | W/(m$^2$ nm) |